Article

Controllable Growth of Graphene Photonic Crystal Fibers with Tunable Optical Nonlinearity

Yi Cheng,[○] Wentao Yu,[○] Jin Xie,[○] Ruoyu Wang, Guang Cui, Xu Cheng, Mengwen Li, Kun Wang, Junliang Li, Zhipei Sun, Ke Chen,* Kaihui Liu,* and Zhongfan Liu*

Cite This: https://doi.org/10.1021/acsphotonics.1c01823
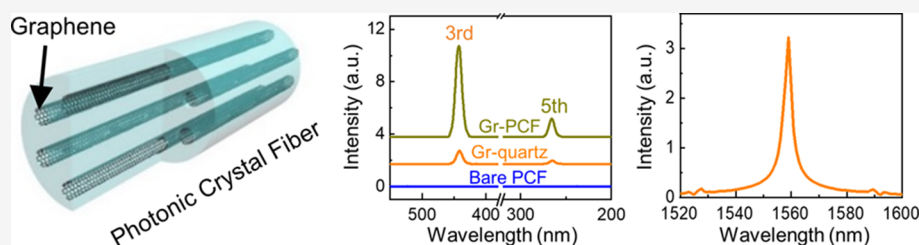
Read Online

ACCESS | Metrics & More | Article Recommendations | Supporting Information

ABSTRACT: The graphene photonic crystal fiber (Gr-PCF), with graphene coated onto the inner hole walls of the fiber, has shown its superiority in various photonic and optoelectronic applications ranging from electro-optic modulators to environmental sensors. However, these applications mainly utilize the linear optical properties of graphene, and its potentials in the nonlinear optical regime are still waiting to be explored. As for the nonlinear applications, the structure and property of Gr-PCF must be precisely manipulated for the tradeoff between nonlinear enhancement and linear absorption loss of graphene. Here, we propose a pressure-controllable chemical vapor deposition strategy to precisely control the uniform fiber length and graphene thickness, realizing the strong and tunable optical nonlinearity of Gr-PCF with acceptable optical loss. Based on the as-fabricated fiber, the nonlinear harmonic generations exhibit nearly one order of magnitude enhancement compared with those of graphene on planar quartz. Moreover, an ultrafast all-fiber laser employing the nonlinear Gr-PCF as a saturable absorber is demonstrated with ∼8 mW output power, ∼2 ps pulse width, and ∼37 MHz repetition frequency. Our results can technically open up an infusive way to precisely engineer the nonlinear properties of graphene optical fibers and broaden their applications in all-fiber photonic and optoelectronic devices.

KEYWORDS: graphene, optical fiber, pressure-controllable chemical vapor deposition, nonlinear harmonic generation, all-fiber laser

INTRODUCTION

Graphene, with an optical nonlinear susceptibility three orders of magnitude higher than conventional bulk optical crystals,[1−4] has shown a promising potential for optical nonlinear applications, such as optical harmonic generation, frequency conversion, and mode-locked laser.[5−7] However, considering the atomic thickness, the absolute light−matter interaction strength for planar graphene is too weak to fulfill the demand of practical applications.[8] To enhance the interaction, great efforts have been made via integrating graphene with an optical fiber, a well-known optical waveguide, such as injecting graphene dispersion into the holes of fiber,[9,10] spinning graphene flakes, or transferring graphene films on D-shaped or tapered fiber.[11−13] Nevertheless, those graphene-integrated optical fibers are still constrained with the short light−matter interaction length, the distortion in the waveguide capacity, or the low production scalability.[9−12]

The porous structured photonic crystal fiber (PCF) provides an advanced platform for integration with versatile functional materials, such as gases, semiconductors, polymers, and liquid crystals and thus expands its functionalities in surface plasmon generation, stimulated Raman scattering, and optical isolation.[14−17] Recently, the emergence of two-dimensional (2D) graphene has attracted a lot of attention in the integration with PCF. In the previous studies, the chemical vapor deposition (CVD) method has been proven to be a plausible route to synthesize graphene PCF (Gr-PCF), which demonstrates enormous potentials in electro-optic modulators and temperature and fluid sensors.[18−20] However, these applications are mainly based on the linear optical properties of graphene. As for the nonlinear applications of Gr-PCF, it requires further advances in realizing the balance between the strong nonlinear light−matter interaction and the undesirable broadband linear
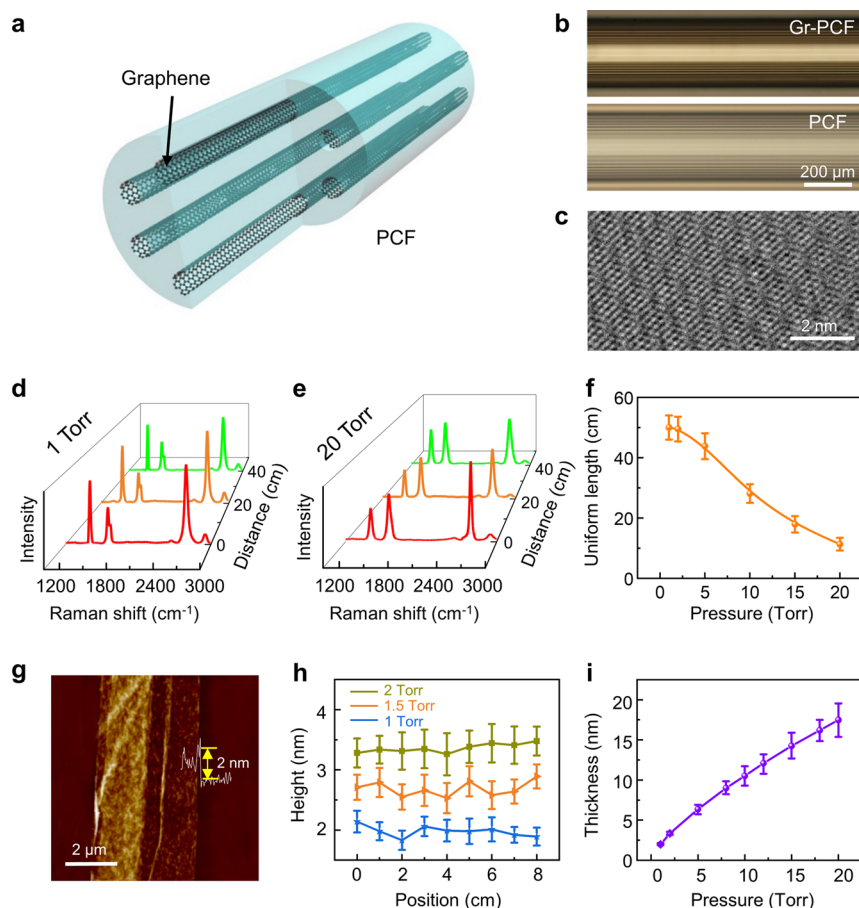
Figure 1. Synthesis of Gr-PCF by the PCCVD method. (a) Schematic of the Gr-PCF structure. (b) Optical image of the Gr-PCF (upper panel) and bare PCF (lower panel). (c) HR-TEM image of the collapsed graphene tube after etching the fiber silica. (d,e) Raman spectra of graphene at different positions (with a distance of 20 cm) of a collapsed graphene tube along the gas flow under the growth pressure of 1 Torr (d) and 20 Torr (e). (f) Variation of uniform fiber length vs the growth pressure. Error bars represent standard deviations from measurements of five samples. (g) AFM image of the collapsed graphene tube. (h) Thickness of graphene tubes along the fiber axis under different growth pressures. The blue star, orange triangle, and dark yellow square represent the fiber sample synthesized under 1, 1.5, and 2 Torr, respectively. Error bars represent standard deviations from measurements of five samples. (i) Average thickness of the graphene changing with the increase of the growth pressure. Error bars represent standard deviations from the measurements of five 50 cm-long samples and 10 different positions with an interval of 5 cm.

absorption loss of graphene, which are significantly influenced by the graphene thickness and the fiber length.[21] When the graphene thickness and fiber length increase, nonlinear light–matter interaction of Gr-PCF increases with the simultaneous increase of the linear absorption loss, leading to the saturation and even degradation of the nonlinear signal. However, precise manipulation of these properties of the as-fabricated Gr-PCF is still challenging, especially considering the difficulties of gas flow control inside the micrometer-sized PCF holes.

Here, we provide a pressure-controllable CVD (PCCVD) strategy to precisely control the uniform fiber length and graphene thickness. As a key parameter for graphene growth, the system pressure can influence the mean free path and fluid state of the reactant molecules inside the microholes. As system pressure increases, the mean free path of the flowing gas decreases with the gradual increase of the molecular collisions in the gaseous phase and the decrease of gas flow velocity, leading to the decrease of the uniform fiber length along the fiber axis. Meanwhile, the concentration of active carbon species also increases, resulting in an increase of graphene thickness.[22−27] Thus, the strong and tunable nonlinearity of Gr-PCF with acceptable linear absorption was achieved for nonlinear optical applications.

■ RESULTS AND DISCUSSION

Gr-PCF with a solid core and regular arranged air holes of ~2.6 μm (Figure 1a) was manufactured by using methane as the carbon precursor under the growth temperature of 1100 °C. The growth of the graphene film inside PCF was directly evinced by the darker contrast of Gr-PCF (Figure 1b, upper panel), compared with the bare PCF (Figure 1b, lower panel). Meanwhile, the intact structure of the as-fabricated Gr-PCF was maintained after the growth, confirmed by the cross-section scanning electron microscopy (SEM) image (Figure S1). Furthermore, the collapsed graphene tubes were obtained after etching the fiber silica, which demonstrated the full coverage of graphene inside the PCF holes (Figures S2 and S3). The high-resolution transmission electron microscopy (HR-TEM) image (Figure 1c) exhibited the regularly arranged crystalline structure with regular Moiré patterns, confirming the high crystallinity of the as-fabricated graphene films.

To clarify the influence of pressure during graphene growth, the pressure-controllable experiments were carried out in the Gr-PCF synthesis. With the increase of growth pressure, the nonuniformity along the fiber axis became much severer (Figure 1d,e). In order to evaluate the uniformity of Gr-PCF, the uniform length of Gr-PCF was defined by Raman
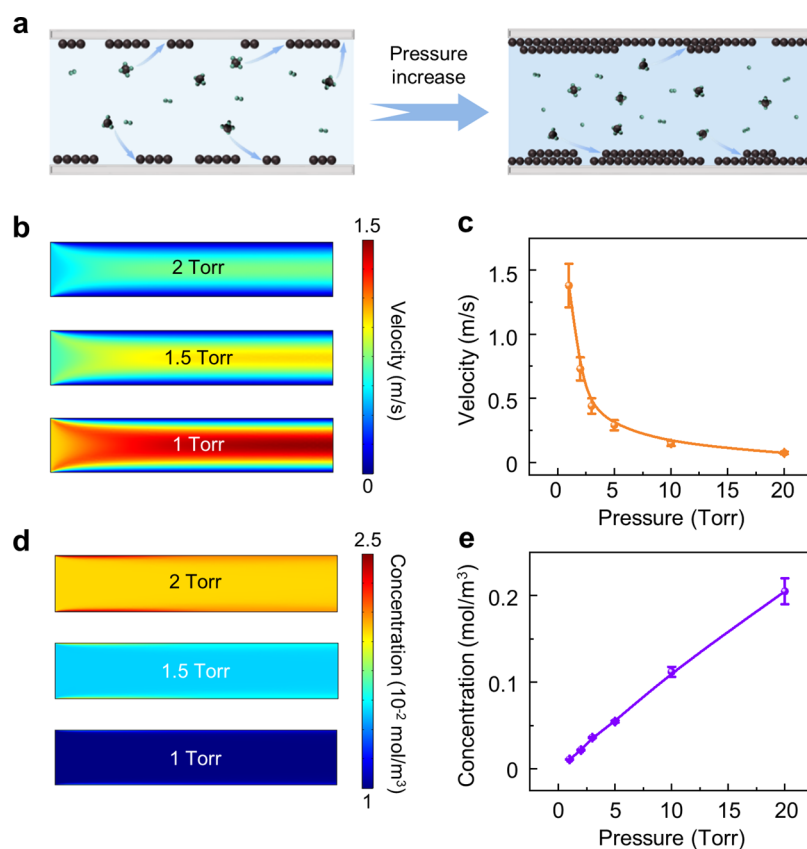
Figure 2. Fluid simulations in the PCF holes. (a) Schematic of graphene growth inside the holes of PCFs with the increase of growth pressure. (b,c) 2D simulated distribution of the gas flow velocity (b) and the calculated average gas flow velocity (c) along the central fiber axis with respect to the growth pressure. Error bars in (c) represent standard deviations of gas flow velocity along the central fiber axis. (d,e) Corresponding simulated methane concentration distribution (d) and its concentration (e) under different growth pressure. Error bars in (e) represent standard deviations of the simulated methane concentration inside the microhole.
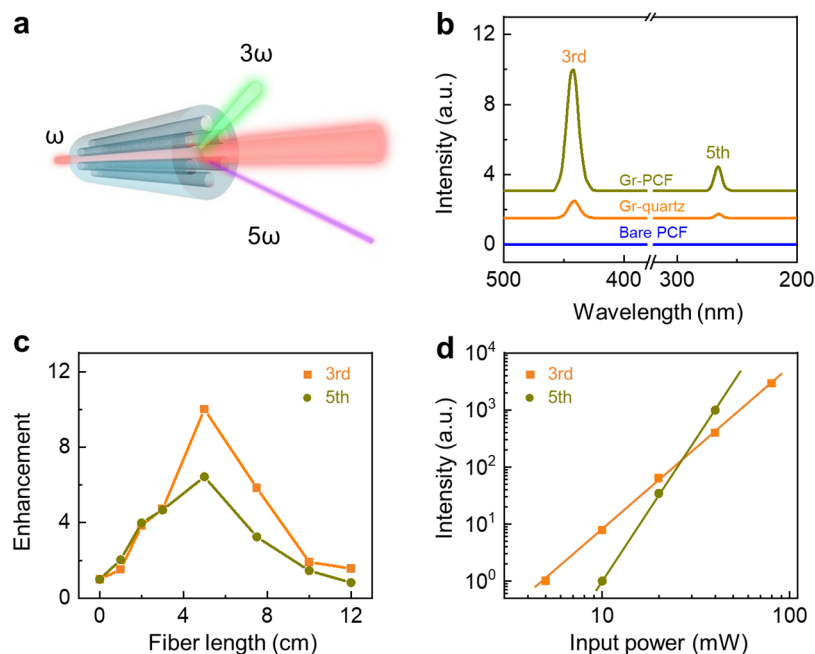
Figure 3. Nonlinear harmonic generation of Gr-PCF. (a) Schematic of third and fifth harmonic generations in Gr-PCF. The different directions are only for better distinguishing the fundamental-mode light, the third- and fifth-order harmonics, which do not represent the real directions of the light. (b) Third and fifth harmonic spectra of Gr-PCF, Gr-quartz, and bare PCF under the excitation of 1330 nm. The fifth harmonic spectra are magnified by 20 times for clarity. (c) Fiber length-dependent third and fifth harmonic generation enhancements compared with that on the plane quartz. (d) Excitation power-dependent third and fifth harmonic intensity of Gr-PCF.

C
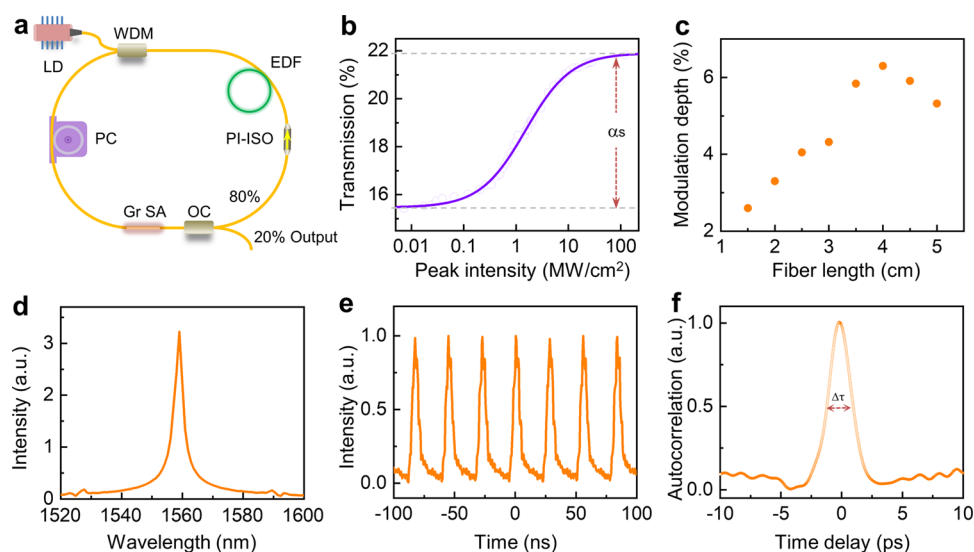
Figure 4. Ultrafast all-fiber laser based on Gr-PCF as a saturable absorber. (a) Schematic of an all-fiber mode-locked laser. (b) Transmission measurement of Gr-PCF with a nonlinear absorption modulation depth of 6.5%. (c) Length-dependent modulation depth of Gr-PCFs. (d–f) Spectrum (d), pulse train (e), and autocorrelation trace (f) of the output laser. The full width at half-maximum of the autocorrelation trace ($\Delta\tau$) is ~2.8 ps, corresponding to a pulse width of ~2 ps, considering the Gaussian convolution factor of 1.414.

characterization, where the variations of the intensity ratio of the 2D- to G-mode Raman peak (I_{2D}/I_G) and full width at half-maximum of the 2D-mode peak ($FWHM_{2D}$) are supposed to be less than 10%.[19,28] As system pressure increased from 1 to 20 Torr, the uniform length of Gr-PCF significantly decreased from ~50 to ~11 cm (Figures 1f and S4). Besides, we specifically manipulated the graphene thickness under pressure ranging from 1 to 2 Torr. The slight variations of I_D/I_G (the intensity ratio of the D- to G-mode Raman peak) and I_{2D}/I_G in Raman spectra (Figure S5) along the fiber axis demonstrated the high uniformity of the as-fabricated Gr-PCF within the uniform length. Atomic force microscopy (AFM) characterizations revealed that the thickness of the etched graphene tube can be uniformly tuned from ~2.0 to ~3.4 nm with the variations of growth pressure in this range (Figure 1g,h). The corresponding graphene layer number increased from the quasi-monolayer to four to five layers by TEM characterizations (Figure S6). When the growth pressure further increases to 20 Torr, the thickness of the graphene tubes can thereby increase to ~17.4 nm (Figures 1i and S7).

The graphene growth atmosphere was further investigated by the fluid simulation, and the graphene growth behaviors are schematically presented in Figure 2a. With the growth pressure changing from 1 to 20 Torr, the fluid state of the reactant gas would transform from the free molecular flow to viscous-molecular transition state (Supporting Information, Note 1), leading to the decrease of the mean free path of the reactant molecular and the gas velocity in the fiber hole (Figure 2b,c), which gave rise to the thus-shortened uniform fiber length (Figure S8).[19,29] Besides, the concentration distribution of the carbon precursors in the microholes significant increases along the central fiber axis from ~0.01 to ~0.21 mol/m³ with the growth pressure increase from 1 to 20 Torr (Figure 2d,e), resulting in the increase of graphene thickness. In brief, the PCCVD strategy can facilitate the precise manipulation of the uniform fiber length and graphene thickness for the fine integration of graphene and PCF.

On the basis of the perfect integration capacity, the Gr-PCF can maintain the intact light waveguide mode and exhibit

strong and tunable light−matter interaction, and it has various potential applications in nonlinear optics. Generally, optical nonlinear applications include the following two parts: (i) nonlinear frequency conversion related to the real part of nonlinear susceptibility, such as nonlinear harmonic generation, parametric process, and supercontinuum generation and (ii) nonlinear absorption related to the imaginary part, such as saturable absorption and related mode-locked pulse generation. By using the as-fabricated Gr-PCF, we synchronously yield the applications in a nonlinear harmonic generation and all-fiber mode-locked laser, providing the potential development direction of Gr-PCF.

As a representative nonlinear application related to the real part of optical nonlinear susceptibility, the nonlinear harmonic generation, such as third and fifth harmonic, was utilized to clarify the excellent optical nonlinearity of Gr-PCF (Figures 3a and S9). Considering the used PCF with endlessly single-mode capacity, the incident laser with a wavelength of ~1330 nm should propagate along the core and interact with the graphene on the inner hole wall. Then, the generated nonlinear harmonics would propagate steadily and output at the fiber end. Considering the high nonlinear susceptibility of the monolayer graphene and the tradeoff between the strong nonlinear light−matter interaction and the inevitable linear absorption loss, the Gr-PCF with monolayer graphene and suitable fiber length was desirable for the nonlinear harmonic generation. As a result, the 5 cm-long Gr-PCF with a quasi-monolayer graphene film demonstrated 10-fold enhancement for third and 6-fold enhancement for the fifth harmonic signal, compared with those of graphene grown on planar quartz (Figure 3b). The nonlinear signals monotonically increased with the fiber length shorter than 5 cm and then decreased with a further elongation of fiber length (Figure 3c). In principle, the nonlinear signal should originate from the interaction between the incident laser and the graphene grown on the inner holes of the PCF and then propagate along the fiber. With the increase of the fiber length, the graphene absorption loss and the phase mismatching effect between the excitation and nonlinear harmonics lead to the saturation

trend. When the fiber length is over 5 cm, the loss of the nonlinear signals is larger than the gain from the harmonic generation, which results in the decrease trend. Meanwhile, a near cubic/quintic dependence of the third/fifth harmonic signal intensity to excitation power was observed as expected in Gr-PCF (Figure 3d), consistent with the theoretical expectation.[30]

In addition, an all-fiber mode-maintaining mode-locked laser, as a typical demonstration of imaginary part-related applications, was also demonstrated based on the designed Gr-PCF as a saturable absorber (SA) at the communication band of ∼1550 nm (Figure 4a). To obtain shorter pulse width and improve the self-starting capability of a mode-locked laser, the Gr-PCF SA with the large nonlinear absorption modulation depth is desirable.[31] Here, the modulation depth (α_s) can be defined as the difference in transmittance under the input laser peak intensity (I) of zero and positive infinity according to the fitted function as $T = 1 - \alpha_{ns} - \frac{\alpha_s}{1 + I/I_{sat}}$,[32] where T is the transmission, α_{ns} is the nonsaturable loss, and I_{sat} is the saturation peak intensity (Figure 4b). By controlling the fiber length and the graphene thickness, the optimal modulation depth was measured as 6.5% with the acceptable saturable transmission of 22% under the 4 cm-long fiber with a quasi-monolayer graphene film (Figures 4c and S10). Subsequently, a passively mode-locked fiber laser was implemented by dispersion management with a near-zero group velocity dispersion (GVD) for the stretched pulse generation.[33] The maximum output power of the pulsed laser is ∼8 mW (under the pump power of 600 mW) with ∼4 nm spectral bandwidth, ∼1559 nm center wavelength (Figure 4d), ∼37 MHz repetition frequency (Figure 4e), and ∼2 ps pulse duration (Figure 4f). Besides, the pulse width could be further compressed to ∼1 ps for the Fourier transform-limited pulse by the GVD compensation outside the cavity, considering the ∼4 nm spectral bandwidth.[34] Via using 55 cm standard single-mode fiber length outside the laser ring for the compensation of the GVD, the output pulse width can be further compressed to ∼1.2 ps (Figure S11). The competitive performance, great capacity of massive production, and the environmental compatibility of the CVD grown Gr-PCF have demonstrated the distinct superiorities compared to the conventional graphene-integrated fibers via transfer or filling methods (Table S1). In addition, compared with other SAs based on carbon nanotubes or transition metal chalcogenides, the graphene can work in a broader wavelength region from ultraviolet to near-infrared.

CONCLUSIONS

In summary, by virtue of the PCCVD method, we successfully synthesized Gr-PCF with controllable thickness and uniform fiber length. Thus, the nonlinear applications, such as nonlinear harmonic generation and all-fiber mode-locked laser, have been realized with a balance between strong nonlinear light−matter interaction and acceptable linear absorption loss. The excellent nonlinear optical performance and massive manufacturing capacity of the as-fabricated Gr-PCF via the PCCVD strategy demonstrate its distinct superiorities compared with that by transfer techniques. In addition, combined with the well-designed structure of the optical fiber, Gr-PCF can be further extended in versatile optical nonlinear applications, such as optical parametric amplification, optical frequency comb, and multi-wavelength mode-locked laser.

METHODS

Synthesis of Gr-PCFs by PCCVD. Before graphene growth, a fiber stripper (T08S13, THORLABS) was utilized to remove the polymer coatings on the surface of the PCFs (∼10 μm solid core diameter and ∼125 μm fiber diameter, NKT Photonics, LMA-10). Then, the naked PCFs were cut with desired lengths using the fiber cutter (CT-50, Fujikura), while maintaining its end face clean. These PCFs were put inside the central zone of a 1-inch quartz tube of a CVD furnace (Thermo Linderberg) along the gas-flow direction. Dozens of Gr-PCFs can be fabricated in a single batch in order to achieve a higher productivity. The CVD chamber was then heated to the desired growth temperature of 1100 °C with the rate of 20 °C/min. For the graphene growth, CH_4 (20 sccm) and H_2 (80 sccm) were introduced to the CVD system for hours. The growth pressure for graphene growth was controlled by a flow valve (MKS 253B) ranging from 0.5 to 20 Torr. After the growth, the as-fabricated Gr-PCFs were naturally cooled down to the room temperature under the mixture gas of hydrogen and argon.

Characterization of Gr-PCFs. Optical images of Gr-PCFs were obtained by a Nikon LV100ND microscope. SEM observations were conducted by FEI Quattro S at 10−20 kV acceleration voltage. Energy-dispersive spectroscopy (EDS) was performed by DigiView/Octane Elect. Raman spectra were obtained with LabRAM HR-800 with a 532 nm laser and 100× objective. AFM was carried out using a Bruker Dimension Icon atomic force microscope to measure graphene thickness on the inner holes of PCFs. HR-TEM characterizations were taken by a FEI Titan Themis G2-300 system with an acceleration voltage of 80 kV. The as-fabricated Gr-PCF was put on the silicon substrates or TEM grids and then immersed into hydrofluoric acid solution (20 wt %) for 6 h. After the dissolution of the silica fiber, the few-layer graphene grown on the wall of the microholes collapsed and overlapped onto the substrates. After being further washed by deionized water and ethanol to remove the residual chemical reagents, the collapsed graphene tubes could be obtained for the Raman, AFM, and HR-TEM characterizations.

Fluid Simulation. Fluid simulations were conducted by the COMSOL's Multiphysics software based on the finite element method. The simulated diameter of the PCF hole was set as 2.6 μm, and the computational mesh arrangement of 26,000 cells was performed with a triangle mesh for the convergence. The reactant gas mass flow was set based on the measurements of the flowmeters (HORIBA METRON, S48 32/HMT) with the set temperature of 1100 °C and the set system pressure based on the flow valve (MKS 253B) measurement. The outlet boundary condition is set based on the performance curve of the mechanical pump in a CVD experiment (Edwards, E2M18).

Measurement of the Harmonic Generation. The excitation laser (1330 nm, 150 fs, 250 kHz) was generated from an optical parameter amplifier (Mira-OPO-9450, Coherent) pumped by high-power Ti-sapphire oscillator (Coherent Vitara-T, Coherent) and focused on the port core of Gr-PCF/bare PCF or graphene on the planar quartz via an objective (Nikon, ×10, NA = 0.25) in the homemade measurement system. During the measurement of the harmonic generation, we applied the same input laser power and the same microscopic objective lens for the same focused spot. A homemade optical image system was used to ensure

the accurate focus for different samples and adjust the signal collection part for the maximum and similar efficiency. The third and fifth harmonic signals were collected by an objective lens via a transmission light path to a spectrograph equipped with an ultraviolet to visible charge-coupled device (DU420A-BU2, Andor) after filtering the excitation laser.

Characterization of Saturable Absorption. A pulsed fiber laser (Origami 15, NKT Photonics) with a center wavelength of ∼1550 nm, pulse width of 150 fs, and repetition frequency of 100 MHz, Origami 15, NKT Photonics) was utilized to measure the saturable absorption ability of Gr-PCF. Then, the input laser was divided by 90%/10% through a fiber optics coupler for real-time monitoring of the power (90% for incident laser and 10% for monitoring). The input fiber (SM-28e+, Corning) was aligned with the Gr-PCF using two sets of microscopies along different directions. By comparing output laser power with the monitoring power, the power dependence transmission could be measured.

Characterization of an All-Fiber Mode-Locked Laser Based on Gr-PCF. A pump laser (976 nm) was coupled into the ring cavity of the fiber laser by using a wavelength-division multiplex (980 nm/1550 nm) and then pumped the gain medium (the 60 cm-long Er-fiber, Er110 4-125, LIEKKI). The laser in the ring cavity could only propagate along one direction by inserting a polarization-independent isolator. The Gr-PCF was integrated into the fiber ring as a SA for mode locking, and the pulsed laser was outputted via a 20% port of the fiber coupler, while the spectrum was optimized by a polarization controller. Considering the similar mode-field size between the used PCF (LMA-10, NKT Photonics) and standard single-mode fiber (SM-28e+, Corning), the insert loss is measured with ∼2 dB, which is acceptable in the all-fiber devices. The total GVD of the fiber ring was 0.0012 ps^2, which was near-zero dispersion, for the dispersion management configuration. The spectrum was measured by a Fourier transform infrared spectrometer (OSA205C, Thorlabs), while the pulse train was monitored via the photodetector (DET08CFC/M, Thorlabs) and the oscilloscope (DS6104, Rigol). The pulse width was obtained by autocorrelation trace measurement via the autocorrelator (Pulsecheck USB 50, APE).

■ ASSOCIATED CONTENT

ⓈI Supporting Information

The Supporting Information is available free of charge at https://pubs.acs.org/doi/10.1021/acsphotonics.1c01823.

Characterizations of Gr-PCF, simulation attenuation and measured modulation depth of Gr-PCF with different graphene layers, calculation of fluid dynamics, and comparisons of ultrafast lasers based on graphene integrated optical fibers by different methods (PDF)

■ AUTHOR INFORMATION

Corresponding Authors

Ke Chen − *Center for the Physics of Low-Dimensional Materials, School of Physics and Electronics, Henan University, Kaifeng 475004, P. R. China; Beijing Graphene Institute (BGI), Beijing 100095, P. R. China;* orcid.org/0000-0003-2384-8437; Email: kchen@henu.edu.cn

Kaihui Liu − *State Key Laboratory for Mesoscopic Physics, Frontiers Science Center for Nano-optoelectronics, School of Physics and Academy for Advanced Interdisciplinary Studies, Collaborative Innovation Center of Quantum Matter, Peking University, Beijing 100871, P. R. China;* orcid.org/0000-0002-8781-2495; Email: khliu@pku.edu.cn

Zhongfan Liu − *Center for Nanochemistry, Beijing Science and Engineering Center for Nanocarbons, Beijing National Laboratory for Molecular Sciences, College of Chemistry and Molecular Engineering, Peking University, Beijing 100871, P. R. China; Beijing Graphene Institute (BGI), Beijing 100095, P. R. China;* orcid.org/0000-0003-0065-7988; Email: zfliu@pku.edu.cn

Authors

Yi Cheng − *Center for Nanochemistry, Beijing Science and Engineering Center for Nanocarbons, Beijing National Laboratory for Molecular Sciences, College of Chemistry and Molecular Engineering, Peking University, Beijing 100871, P. R. China*

Wentao Yu − *State Key Laboratory for Mesoscopic Physics, Frontiers Science Center for Nano-optoelectronics, School of Physics, Peking University, Beijing 100871, P. R. China; Institute of Interdisciplinary Physical Sciences, School of Science, Nanjing University of Science and Technology, Nanjing 210094, P. R. China*

Jin Xie − *State Key Laboratory for Mesoscopic Physics, Frontiers Science Center for Nano-optoelectronics, School of Physics and Academy for Advanced Interdisciplinary Studies, Collaborative Innovation Center of Quantum Matter, Peking University, Beijing 100871, P. R. China*

Ruoyu Wang − *Center for Nanochemistry, Beijing Science and Engineering Center for Nanocarbons, Beijing National Laboratory for Molecular Sciences, College of Chemistry and Molecular Engineering, Peking University, Beijing 100871, P. R. China*

Guang Cui − *Center for Nanochemistry, Beijing Science and Engineering Center for Nanocarbons, Beijing National Laboratory for Molecular Sciences, College of Chemistry and Molecular Engineering, Peking University, Beijing 100871, P. R. China*

Xu Cheng − *State Key Laboratory for Mesoscopic Physics, Frontiers Science Center for Nano-optoelectronics, School of Physics, Peking University, Beijing 100871, P. R. China*

Mengwen Li − *Beijing Graphene Institute (BGI), Beijing 100095, P. R. China*

Kun Wang − *Center for Nanochemistry, Beijing Science and Engineering Center for Nanocarbons, Beijing National Laboratory for Molecular Sciences, College of Chemistry and Molecular Engineering, Peking University, Beijing 100871, P. R. China*

Junliang Li − *Beijing Graphene Institute (BGI), Beijing 100095, P. R. China*

Zhipei Sun − *Department of Electronics and Nanoengineering, Aalto University, Espoo 02150, Finland;* orcid.org/0000-0002-9771-5293

Complete contact information is available at:
https://pubs.acs.org/10.1021/acsphotonics.1c01823

Author Contributions

○Y.C., W.Y., and J.X. contributed equally to this work.

■ REFERENCES

(1) Hendry, E.; Hale, P. J.; Moger, J.; Savchenko, A. K.; Mikhailov, S. A. Coherent Nonlinear Optical Response of Graphene. *Phys. Rev. Lett.* **2010**, *105*, No. 097401.

(2) Hong, S. Y.; Dadap, J. I.; Petrone, N.; Yeh, P. C.; Hone, J.; Osgood, R. M. Optical Third-Harmonic Generation in Graphene. *Phys. Rev. X* **2013**, *3*, No. 021014.

(3) Cheng, J. L.; Vermeulen, N.; Sipe, J. E. Third Order Optical Nonlinearity of Graphene. *New J. Phys.* **2014**, *16*, No. 053014.

(4) Chang, C.; Chen, W.; Chen, Y.; Chen, Y.; Chen, Y.; Ding, F.; Fan, C.; Jin Fan, H.; Fan, Z.; Gong, C.; Gong, Y.; He, Q.; Hong, X.; Hu, S.; Hu, W.; Huang, W.; Huang, Y.; Ji, W.; Li, D.; Li, L.-J.; Li, Q.; Lin, L.; Ling, C.; Liu, M.; Liu, N.; Liu, Z.; Ping Loh, K.; Ma, J.; Miao, F.; Peng, H.; Shao, M.; Song, L.; Su, S.; Sun, S.; Tan, C.; Tang, Z.; Wang, D.; Wang, H.; Wang, J.; Wang, X.; Wang, X.; Wee, A. T. S.; Wei, Z.; Wu, Y.; Wu, Z.-S.; Xiong, J.; Xiong, Q.; Xu, W.; Yin, P.; Zeng, H.; Zeng, Z.; Zhai, T.; Zhang, H.; Zhang, H.; Zhang, Q.; Zhang, T.; Zhang, X.; Zhao, L.-D.; Zhao, M.; Zhao, W.; Zhao, Y.; Zhou, K.-G.; Zhou, X.; Zhou, Y.; Zhu, H.; Zhang, H.; Liu, Z. Recent Progress on Two-Dimensional Materials. *Acta Phys.-Chim. Sin.* **2021**, *37*, No. 2108017.

(5) Yoshikawa, N.; Tamaya, T.; Tanaka, K. High-Harmonic Generation in Graphene Enhanced by Elliptically Polarized Light Excitation. *Science* **2017**, *356*, 736−738.

(6) Gu, T.; Petrone, N.; McMillan, J. F.; van der Zande, A.; Yu, M.; Lo, G. Q.; Kwong, D. L.; Hone, J.; Wong, C. W. Regenerative Oscillation and Four-Wave Mixing in Graphene Optoelectronics. *Nat. Photonics* **2012**, *6*, 554−559.

(7) Sun, Z. P.; Hasan, T.; Torrisi, F.; Popa, D.; Privitera, G.; Wang, F. Q.; Bonaccorso, F.; Basko, D. M.; Ferrari, A. C. Graphene Mode-Locked Ultrafast Laser. *ACS Nano* **2010**, *4*, 803−810.

(8) Nair, R. R.; Blake, P.; Grigorenko, A. N.; Novoselov, K. S.; Booth, T. J.; Stauber, T.; Peres, N. M. R.; Geim, A. K. Fine Structure Constant Defines Visual Transparency of Graphene. *Science* **2008**, *320*, 1308−1308.

(9) Choi, S. Y.; Cho, D. K.; Song, Y. W.; Oh, K.; Kim, K.; Rotermund, F.; Yeom, D. I. Graphene-Filled Hollow Optical Fiber Saturable Absorber for Efficient Soliton Fiber Laser Mode-Locking. *Opt. Express* **2012**, *20*, 5652−5657.

(10) Lin, Y.-H.; Yang, C.-Y.; Liou, J.-H.; Yu, C.-P.; Lin, G.-R. Using Graphene Nano-Particle Embedded in Photonic Crystal Fiber for Evanescent Wave Mode-Locking of Fiber Laser. *Opt. Express* **2013**, *21*, 16763−16776.

(11) Bao, Q.; Zhang, H.; Wang, B.; Ni, Z.; Lim, C. H. Y. X.; Wang, Y.; Tang, D. Y.; Loh, K. P. Broadband Graphene Polarizer. *Nat. Photonics* **2011**, *5*, 411−415.

(12) Li, W.; Chen, B.; Meng, C.; Fang, W.; Xiao, Y.; Li, X.; Hu, Z.; Xu, Y.; Tong, L.; Wang, H.; Liu, W.; Bao, J.; Shen, Y. R. Ultrafast All-Optical Graphene Modulator. *Nano Lett.* **2014**, *14*, 955−959.

(13) Lee, E. J.; Choi, S. Y.; Jeong, H.; Park, N. H.; Yim, W.; Kim, M. H.; Park, J.-K.; Son, S.; Bae, S.; Kim, S. J.; Lee, K.; Ahn, Y. H.; Ahn, K. J.; Hong, B. H.; Park, J.-Y.; Rotermund, F.; Yeom, D.-I. Active Control

(14) Markos, C.; Travers, J. C.; Abdolvand, A.; Eggleton, B. J.; Bang, O. Hybrid Photonic-Crystal Fiber. *Rev. Mod. Phys.* **2017**, *89*, No. 045003.

(15) Benabid, F.; Knight, J. C.; Antonopoulos, G.; Russell, P. S. J. Stimulated Raman Scattering in Hydrogen-Filled Hollow-Core Photonic Crystal Fiber. *Science* **2002**, *298*, 399−402.

(16) Markos, C.; Vlachos, K.; Kakarantzas, G. Guiding and Thermal Properties of a Hybrid Polymer-Infused Photonic Crystal Fiber. *Opt. Mater. Express* **2012**, *2*, 929−941.

(17) Wu, T.; Shao, Y.; Wang, Y.; Cao, S. Q.; Cao, W. P.; Zhang, F.; Liao, C. R.; He, J.; Huang, Y. J.; Hou, M. X.; Wang, Y. P. Surface Plasmon Resonance Biosensor Based on Gold-Coated Side-Polished Hexagonal Structure Photonic Crystal Fiber. *Opt. Express* **2017**, *25*, 20313−20322.

(18) Cheng, X.; Zhou, X.; Huang, C.; Liu, C.; Ma, C. J.; Hong, H.; Yu, W. T.; Liu, K. H.; Liu, Z. F. Tunable and Highly Sensitive Temperature Sensor Based on Graphene Photonic Crystal Fiber. *Chin. Phys. B* **2021**, *30*, 118103.

(19) Chen, K.; Zhou, X.; Cheng, X.; Qiao, R.; Cheng, Y.; Liu, C.; Xie, Y.; Yu, W.; Yao, F.; Sun, Z.; Wang, F.; Liu, K.; Liu, Z. Graphene Photonic Crystal Fibre with Strong and Tunable Light−Matter Interaction. *Nat. Photonics* **2019**, *13*, 754−759.

(20) Qiu, H. W.; Xu, S. C.; Jiang, S. Z.; Li, Z.; Chen, P. X.; Gao, S. S.; Zhang, C.; Feng, D. J. A Novel Graphene-Based Tapered Optical Fiber Sensor for Glucose Detection. *Appl. Surf. Sci.* **2015**, *329*, 390−395.

(21) Yamashita, S.; Martinez, A.; Xu, B. Short Pulse Fiber Lasers Mode-Locked by Carbon Nanotubes and Graphene. *Opt. Fiber Technol.* **2014**, *20*, 702−713.

(22) Li, G.; Huang, S. H.; Li, Z. Gas-Phase Dynamics in Graphene Growth by Chemical Vapour Deposition. *Phys. Chem. Chem. Phys.* **2015**, *17*, 22832−22836.

(23) Bhaviripudi, S.; Jia, X.; Dresselhaus, M. S.; Kong, J. Role of Kinetic Factors in Chemical Vapor Deposition Synthesis of Uniform Large Area Graphene Using Copper Catalyst. *Nano Lett.* **2010**, *10*, 4128−4133.

(24) Cho, J. H.; Na, S. R.; Park, S.; Akinwande, D.; Liechti, K. M.; Cullinan, M. A. Controlling the Number of Layers in Graphene Using the Growth Pressure. *Nanotechnology* **2019**, *30*, 235602.

(25) Liu, Q.; Gong, Y.; Wilt, J. S.; Sakidja, R.; Wu, J. Synchronous Growth of AB-Stacked Bilayer Graphene on Cu by Simply Controlling Hydrogen Pressure in CVD Process. *Carbon* **2015**, *93*, 199−206.

(26) Cui, G.; Cheng, Y.; Liu, C.; Huang, K.; Li, J.; Wang, P.; Duan, X.; Chen, K.; Liu, K.; Liu, Z. Massive Growth of Graphene Quartz Fiber as a Multifunctional Electrode. *ACS Nano* **2020**, *14*, 5938−5945.

(27) Cheng, Y.; Wang, K.; Qi, Y.; Liu, Z. Chemical Vapor Deposition Method for Graphene Fiber Materials. *Acta Phys.-Chim. Sin.* **2022**, *38*, No. 2006046.

(28) Chen, X. D.; Chen, Z.; Jiang, W. S.; Zhang, C.; Sun, J.; Wang, H.; Xin, W.; Lin, L.; Priydarshi, M. K.; Yang, H.; Liu, Z. B.; Tian, J. G.; Zhang, Y.; Zhang, Y.; Liu, Z. Fast Growth and Broad Applications of 25-Inch Uniform Graphene Glass. *Adv. Mater.* **2017**, *29*, No. 1603428.

(29) Wang, H.; Xu, X.; Li, J.; Lin, L.; Sun, L.; Sun, X.; Zhao, S.; Tan, C.; Chen, C.; Dang, W.; Ren, H.; Zhang, J.; Deng, B.; Koh, A. L.; Liao, L.; Kang, N.; Chen, Y.; Xu, H.; Ding, F.; Liu, K.; Peng, H.; Liu, Z. Surface Monocrystallization of Copper Foil for Fast Growth of Large Single-Crystal Graphene under Free Molecular Flow. *Adv. Mater.* **2016**, *28*, 8968−8974.

(30) Shen, Y.-R. *The Principles of Nonlinear Optics*; Wiley: New York, 1984.

(31) Liu, H. H.; Chow, K. K. Enhanced Stability of Dispersion-Managed Mode-Locked Fiber Lasers with near-Zero Net Cavity Dispersion by High-Contrast Saturable Absorbers. *Opt. Lett.* **2014**, *39*, 150−153.

(32) Wang, F.; Rozhin, A.; Scardaci, V.; Sun, Z.; Hennrich, F.; White, I.; Milne, W. I.; Ferrari, A. C. Wideband-Tuneable, Nanotube Mode-Locked, Fibre Laser. *Nat. Nanotechnol.* **2008**, *3*, 738.

(33) Ilday, F. O.; Wise, F. W.; Sosnowski, T. High-Energy Femtosecond Stretched-Pulse Fiber Laser with a Nonlinear Optical Loop Mirror. *Opt. Lett.* **2002**, *27*, 1531−1533.

(34) Lefort, C.; Mansuryan, T.; Louradour, F.; Barthelemy, A. Pulse Compression and Fiber Delivery of 45 Fs Fourier Transform Limited Pulses at 830 Nm. *Opt. Lett.* **2011**, *36*, 292−294.